

Dendritic encoding of sensory stimuli controlled by deep cortical interneurons

Masanori Murayama¹, Enrique Pérez-García¹, Thomas Nevian¹, Tobias Bock¹, Walter Senn¹ & Matthew E. Larkum¹

The computational power of single neurons is greatly enhanced by active dendritic conductances¹ that have a large influence on their spike activity^{2–4}. In cortical output neurons such as the large pyramidal cells of layer 5 (L5), activation of apical dendritic calcium channels leads to plateau potentials that increase the gain of the input/output function⁵ and switch the cell to burst-firing mode^{6–9}. The apical dendrites are innervated by local excitatory and inhibitory inputs as well as thalamic^{10–13} and corticocortical projections^{14–16}, which makes it a formidable task to predict how these inputs influence active dendritic properties *in vivo*. Here we investigate activity in populations of L5 pyramidal dendrites of the somatosensory cortex in awake and anaesthetized rats following sensory stimulation using a new fibre-optic method¹⁷ for recording dendritic calcium changes. We show that the strength of sensory stimulation is encoded in the combined dendritic calcium response of a local population of L5 pyramidal cells in a graded manner. The slope of the stimulus–response function was under the control of a particular subset of inhibitory neurons activated by synaptic inputs predominantly in L5. Recordings from single apical tuft dendrites *in vitro* showed that activity in L5 pyramidal neurons disynaptically coupled via interneurons directly blocks the initiation of dendritic calcium spikes in neighbouring pyramidal neurons. The results constitute a functional description of a cortical microcircuit in awake animals that relies on the active properties of L5 pyramidal dendrites and their very high sensitivity to inhibition. The microcircuit is organized so that local populations of apical dendrites can adaptively encode bottom-up sensory stimuli linearly across their full dynamic range.

To explore how dendritic activity encodes sensory input *in vivo*, we used a microendoscopic technique (the ‘periscope’ method¹⁷) ideal for recording from local populations of L5 pyramidal dendrites in anaesthetized and awake animals (Fig. 1a, Methods). This method provides calcium fluorescence signals exclusively from pyramidal apical tuft dendrites by combining two approaches: specific loading of L5 pyramidal dendrites and horizontal imaging of the upper three layers of cortex (Fig. 1a). Fluorescence responses to sensory stimuli were recorded from populations of L5 bolus-loaded dendrites that were not detectable using two-photon imaging from individual dendrites¹⁸ ($n = 6$, data not shown; see also Methods). This method has a high sensitivity to dendritic activity and can be easily applied to awake, freely moving animals.

Air-puff stimulation of the hindlimb under urethane anaesthesia produced biphasic responses in dendrites of the contralateral hindlimb area of the primary somatosensory cortex (Fig. 1b, black). This dendritic population response could be blocked completely by the application of the Ca²⁺ channel blocker Cd²⁺ to the cortical surface (Fig. 1b, grey), leaving no detectable movement artefacts. Application of the GABA_A (GABA, γ -aminobutyric acid) receptor antagonist, gabazine, to the cortical surface increased the first component of the dendritic

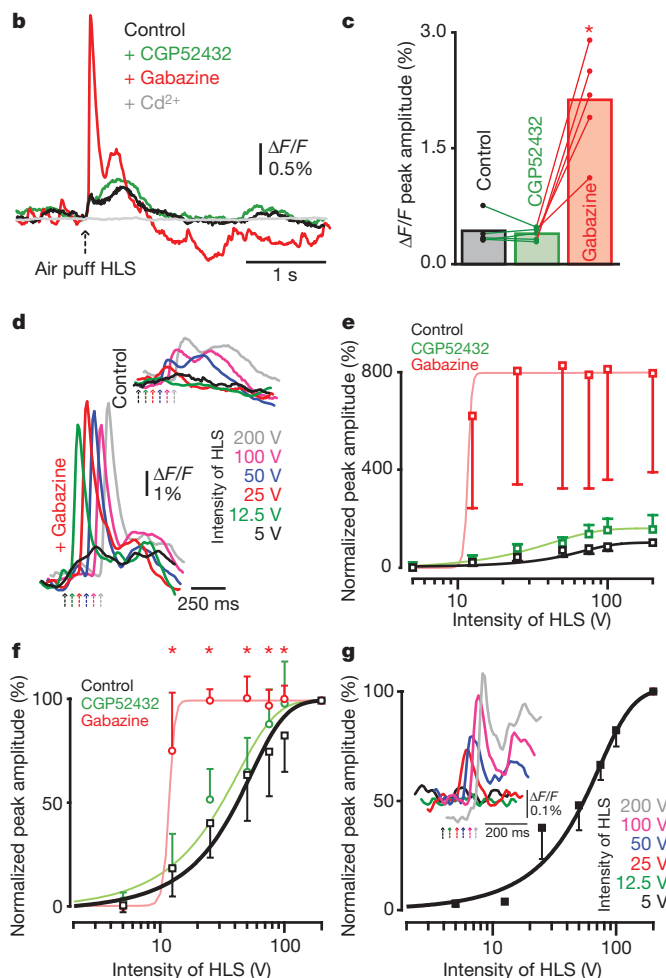
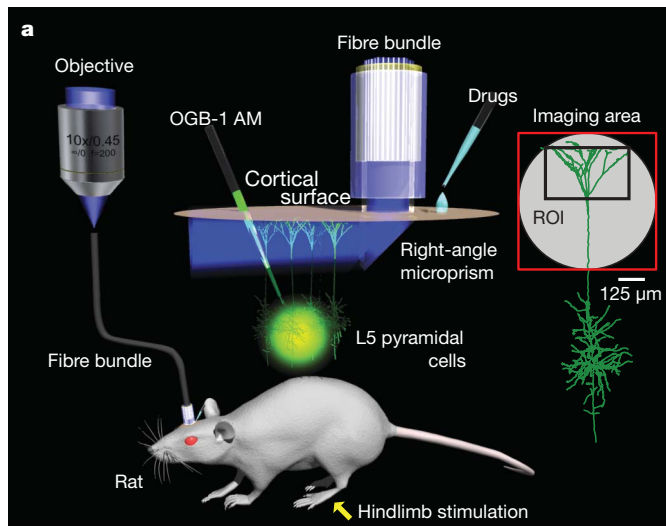
population response approximately fivefold ($0.42 \pm 16\%$ versus $2.12 \pm 0.60\%$ (all data given as mean \pm s.d.), $P < 0.05$, $n = 5$; Fig. 1b, c, red), whereas the GABA_B receptor antagonist CGP52432 did not change this component ($0.42 \pm 0.16\%$ versus $0.38 \pm 0.07\%$, $P = 0.29$, $n = 5$; Fig. 1b, c, green). Throughout this study we focused on the factors influencing the increase in the initial component of calcium influx into the dendrites modulated by GABA_A receptors.

We investigated the dendritic encoding of stimulus strength using single electrical stimuli to the hindlimb, for which the strength could be reliably and precisely determined. Increasing stimulus strength under urethane anaesthesia resulted in a progressive increase in the population dendritic calcium response ($n = 21$; Fig. 1d; see Supplementary Fig. 1 for $\Delta F/F$ peak amplitude). Blockade of GABA receptors dramatically increased the dendritic population response ($n = 6$; Fig. 1d, e, red), possibly also because of runaway cortical excitation. Blockade of GABA_B receptors alone had very little effect ($n = 6$; Fig. 1e, green). Normalization to the maximal dendritic response in each condition revealed that the responses to increasing stimulus strength were nearly linear under control conditions but highly nonlinear (‘all or none’) without GABA_A receptor activity (Fig. 1f).

Conscious perception involves a combination of feed-forward and feedback processes¹⁹ that may specifically influence dendritic encoding. To examine dendritic sensory-evoked responses in awake animals, we used a custom-built head mount to stabilize the fibre-optic cable¹⁷. As in the anaesthetized state, we found that increasing stimulus strength resulted in a graded increase in the population dendritic calcium response ($n = 3$; Fig. 1g). This shows that the mechanisms controlling the linear encoding of dendritic responses to sensory stimulus strength are not affected by anaesthesia. Thus, we continued our experiments to understand in detail what neural mechanisms underlie the change in linearity and dynamic range in anaesthetized animals.

We next investigated the source of dendritic Ca²⁺. Application of D(-)-2-amino-5-phosphonovaleric acid (APV, to block NMDA receptors) to the cortical surface did not alter the amplitude of the dendritic population signal, indicating negligible contribution by subthreshold Ca²⁺ entry (that is, excitatory postsynaptic potentials (EPSPs)) as shown previously¹⁷ ($P > 0.1$, $n = 6$; Supplementary Fig. 2). However, actively propagated action potentials from the soma into the apical dendrite can cause moderate increases in intracellular calcium concentration ($[Ca^{2+}]_i$), and dendritic Ca²⁺ spikes cause a large signal that is easily detectable¹⁷. There was no way to directly estimate action potential firing with the periscope method, so we tested the contribution of back-propagating action potentials (BPAPs) to the sensory-evoked dendritic calcium signals by injecting TTX (a Na⁺ channel blocker) into L5 (Fig. 2a). Surprisingly, blocking activity in L5 and preventing BPAPs did not decrease the dendritic signal but rather increased it threefold ($1.2 \pm 0.61\%$ versus

¹Physiologisches Institut, Universität Bern, Bühlplatz 5, CH-3012 Bern, Switzerland.



$3.3 \pm 0.95\%$, $P < 0.05$, $n = 5$; Fig. 2b, e) and changed the biphasic nature of the dendritic response. This result shows first that the large calcium responses detected are dependent on neither dendritic BPAPs nor axonal action potentials and second that an additional TTX-sensitive mechanism in L5 suppresses dendritic $[Ca^{2+}]_i$.

The most likely explanation is that TTX also blocked some inhibitory neurons in L5. Recent studies *in vitro* have shown that inhibition of pyramidal dendrites can be evoked by activation of dendrite-targeting Martinotti interneurons by neighbouring pyramidal neurons^{20,21}. To test this possibility, we suppressed the activation of this form of disinaptic inhibition by local injection of CNQX (an antagonist of α -amino-3-hydroxy-5-methyl-4-isoxazole propionic acid (AMPA)

Figure 1 | Graded dendritic population Ca^{2+} responses to somatosensory inputs in anaesthetized and awake rats. **a**, Sketch of the experimental design using the periscope for recording specifically from the apical tuft dendrites of L5 neocortical pyramidal neurons¹⁷. Right: reconstructed pyramidal cell from *in vitro* experiments, demonstrating the typical regions of the dendritic tree within the imaging area. **b**, Averaged dendritic Ca^{2+} population signals (relative fluorescence change, $\Delta F/F$; 15 trials) recorded with the periscope following contralateral hindlimb stimulation with an air puff in anaesthetized rats ($1 \mu M$ CGP52432, $3 \mu M$ gabazine and $1 mM$ Cd^{2+} applied to cortical surface). **c**, Summary of **b** ($n = 5$). Circles show the experiments and bars indicate their averages. **d**, Top: Averaged traces (15 trials) showing increase of dendritic Ca^{2+} signals following increase in contralateral electrical stimulation (arrows indicate the stimulus timing, time-shifted for clarity) of the hindlimb with increasing intensities (5–200 V) under control conditions. Bottom: same, after blockade of all GABA receptors. **e**, Summary of **d** ($n = 21$ for control, $n = 6$ for CGP52432 and gabazine; unpaired *t*-tests) fitted with sigmoidal curves with normalized data to maximal control value (200 V). **f**, Summary of **d** with data normalized to maximum in each condition (200 V). **g**, Summary of awake experiments ($n = 3$). Inset, averaged traces of dendritic Ca^{2+} signals in an awake animal. HLS, hindlimb stimulation; ROI, region of interest. * $P < 0.05$. Error bars, s.d.

receptors and kainate receptors) to L5 (see also Fig. 3). Again, the combined dendritic signal increased ($0.61 \pm 0.19\%$ versus $0.99 \pm 0.36\%$, $P < 0.05$, $n = 5$; Fig. 2c, f). Even more importantly, blockade of both L5 activity using TTX and disinaptic connectivity using CNQX had exactly the same effect on the slope of the dendritic response curve as a function of stimulus strength (Fig. 2h; see Supplementary Fig. 3 for $\Delta F/F$ peak amplitude). We conclude that deep cortical interneurons control dendritic encoding of sensory inputs.

This conclusion was further supported by the counterintuitive action of gabazine when applied locally to L5, which decreased the dendritic Ca^{2+} signal by nearly 40% ($0.76 \pm 0.46\%$ versus $0.45 \pm 0.30\%$, $P < 0.05$, $n = 5$; Fig. 2d, g, h). This is consistent with the hypothesis that disinhibition of L5 cells leads to an increase in dendritic inhibition in the upper layers. Moreover, muscimol (a GABA_A receptor agonist) application to L5 increased the signals evoked by hindlimb stimulations ($0.59 \pm 0.36\%$ versus $0.78 \pm 0.46\%$, $P < 0.05$, $n = 4$; Fig. 2i), whereas muscimol application to layer 1 (L1) decreased dendritic Ca^{2+} signals ($0.89 \pm 0.47\%$ versus $0.63 \pm 0.39\%$, $P < 0.05$, $n = 4$; Fig. 2i). This experiment suggests that inhibition is mainly dendritic, not perisomatic, which was confirmed with muscimol *in vitro* ($n = 3$, Supplementary Fig. 4). Last, these experiments demonstrate that this form of cortical inhibition predominates over increased firing in pyramidal neurons and increases in recurrent activity.

We next investigated the mechanisms underlying inhibitory control of dendritic activity. For this, we examined whether disynaptically evoked inhibition is sufficient to block dendritic Ca^{2+} spikes. We performed triple-patch recordings *in vitro* from pairs of disynaptically coupled L5 pyramidal neurons²⁰ (Fig. 3a) with the third recording in the dendritic Ca^{2+} spike initiation zone 500–800 μm from the cell body ($n = 3$, Fig. 3a). Trains of 18–20 action potentials at 80–100 Hz in the presynaptic pyramidal neuron evoked disynaptic dendritic inhibition (Fig. 3b). Dendritic Ca^{2+} spikes evoked with dendritic current injection (Fig. 3c) could be completely abolished by the disynaptically evoked dendritic inhibition in an all-or-none fashion (Fig. 3d). The same phenomenon could be observed with calcium imaging of the Ca^{2+} spike initiation zone. Disynaptically evoked inhibition severely reduced the Ca^{2+} fluorescence due to Ca^{2+} spikes into this region evoked with high-frequency trains of back-propagating action potentials²² ($23.0 \pm 19.8\%$, $P < 0.05$, $n = 3$; Fig. 3e–g; for details, see Supplementary Fig. 5). The effect of disynaptic inhibition was blocked by local application of CNQX to L5 analogous to the *in vivo* experiments ($n = 3$). The strongest blockade of inhibition occurred when CNQX was puffed close to L5 ($n = 3$, Fig. 3h–j), implying that most of the disynaptic dendritic inhibition is evoked by cells in lower cortical layers.

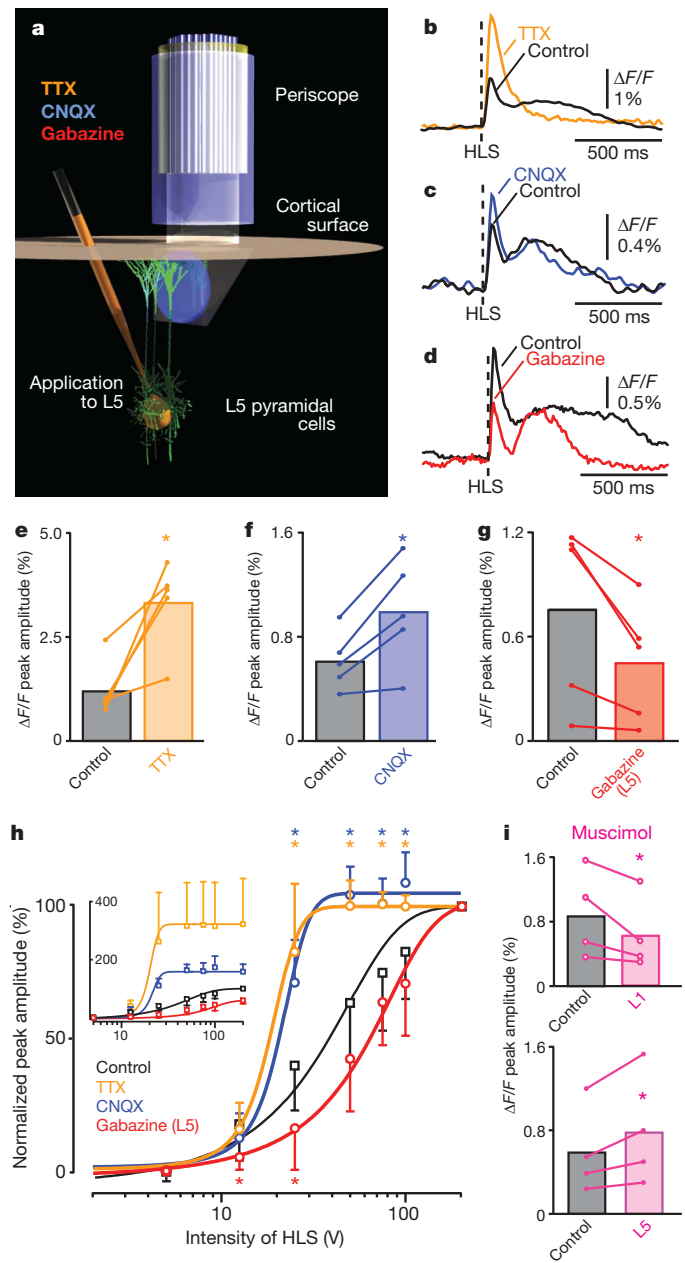


Figure 2 | Deep-layer control of dendritic activity. **a**, Sketch showing local application of tetrodotoxin (TTX, 3 μ M), 6-cyano-7-nitroquinoline-2,3-dione (CNQX, 100 μ M) and gabazine (1 μ M) injected into L5. **b–d** Averaged responses (15 trials) in single animals. **e–g**, Summary of **b–d** ($n = 5$ for each drug). **h**, Responses (normalized to maximum of each condition) versus stimulus strength in control ($n = 21$), with TTX ($n = 5$), CNQX ($n = 5$) and gabazine ($n = 5$). Asterisks indicate significance with unpaired t -tests. Inset, data normalized to control. **i**, Summary of muscimol injection to L1 (top, $n = 4$) and to L5 (bottom, $n = 4$). Application of normal rat ringer to L5 and L1 did not change evoked Ca^{2+} signals ($0.83 \pm 0.76\%$ for control versus $0.76 \pm 0.49\%$ for L5 and $0.77 \pm 0.46\%$ for L1, $n = 3$). * $P < 0.05$. Error bars, s.d.

The experiments show that very specific cortical microcircuitry is involved in determining the responsiveness of apical dendrites of L5 pyramidal neurons (Fig. 4a). Both the *in vivo* and the *in vitro* data suggest that individual dendritic Ca^{2+} signals contribute to the population responses by means of all-or-none Ca^{2+} spikes consistent with previous recordings *in vivo*^{8,23}, and that the inhibition of dendritic Ca^{2+} spikes is also all or none^{24,25}. To investigate how the microcircuitry shapes the grading of the dendritic population response, we modelled a population of two-compartment pyramidal neurons⁵

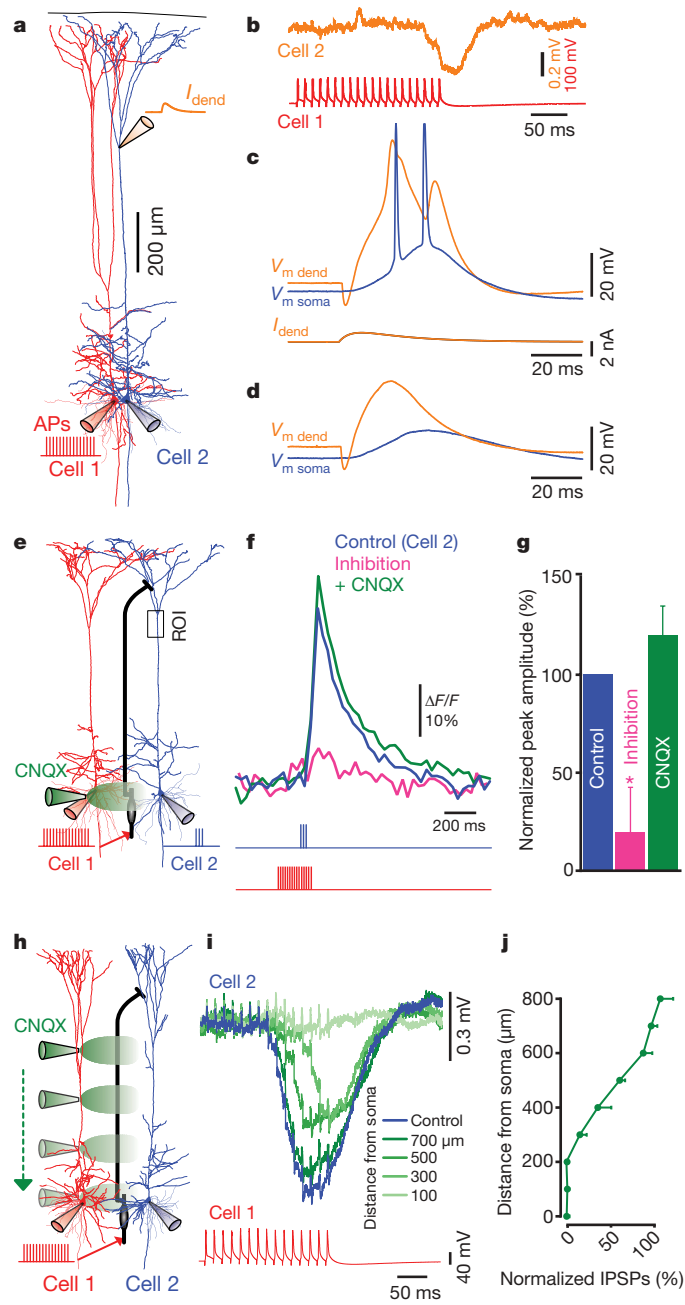


Figure 3 | Disynaptic inhibition blocks dendritic Ca^{2+} spikes *in vitro*. **a**, Experimental diagram showing reconstructed L5 somatosensory pyramidal neurons and recording sites. **b**, Averaged disynaptically evoked inhibitory postsynaptic potential (IPSP) (15 sweeps). **c**, Dendritic Ca^{2+} spike ($V_{m \text{ dend}}$) evoked by dendritic current injection (I_{dend}) caused a burst of somatic action potentials ($V_{m \text{ soma}}$). **d**, Same as **c**, but with disynaptic inhibition. **e**, Experimental diagram. Pyramidal neurons were artificially separated and the putative interneuron (black) added schematically. Cell 2 was filled with OGB-1 (100 μ M) and Ca^{2+} fluorescence ($\Delta F/F$) measured at a distal ROI. CNQX (20 μ M) was applied 100 μ m from the soma. **f**, Ca^{2+} fluorescence transients (blue) were blocked by disynaptic inhibition (pink) and recovered with local application of CNQX (green). **g**, Summary of **f** ($n = 3$). **h**, Experimental diagram. CNQX was applied at nine locations 100 μ m apart in the vertical axis. **i**, Averaged IPSP (30 sweeps) recorded in cell 2 evoked by a train of presynaptic action potentials in cell 1. **j**, Summary of **i** ($n = 3$). AP, action potential. * $P < 0.05$. Error bars, s.d.

receiving distributed feed-forward and feedback excitation and inhibition (Fig. 4b; see Methods and Supplementary Information, model description). The distribution of Ca^{2+} spike thresholds in the dendritic compartments (Fig. 4c, d, green) was chosen to allow for a steep all-or-none Ca^{2+} population response when dendritic

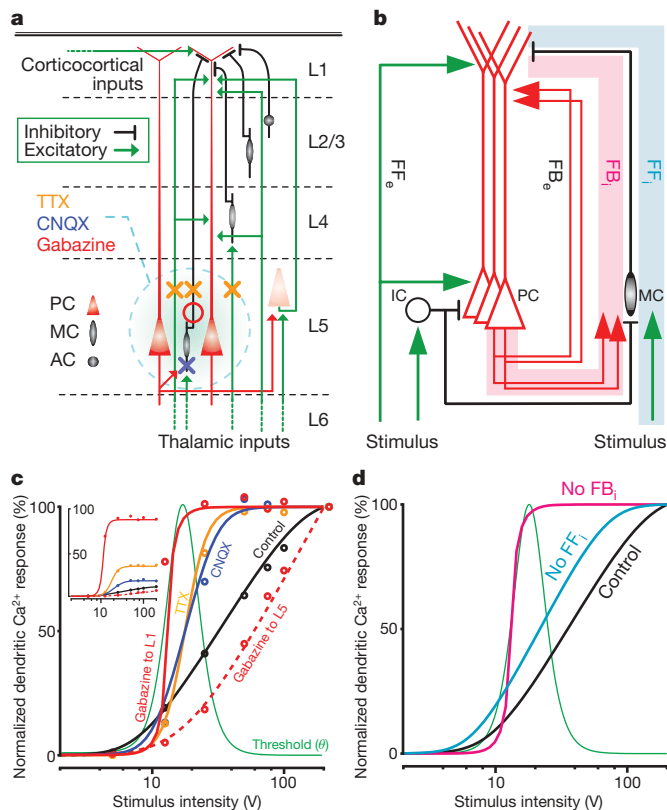


Figure 4 | Model of microcircuitry with all-or-none dendritic Ca^{2+} spikes.

a, Diagram of cortical circuitry. The blue shaded region indicates the elements in the circuit affected by TTX, CNQX and gabazine. PC, pyramidal cell; MC, Martinotti cell; AC, aspiny cell. **b**, Model microcircuitry with a population of two-compartment pyramidal neurons with all-or-none dendritic Ca^{2+} events and four major classes of dendritic inputs (FF_e , feed-forward excitation; FF_i , feed-forward inhibition; FB_e , feedback excitation; FB_i , feedback inhibition; Blue and green arrows, excitation; black lines, inhibition). Dendritic feed-forward inhibition and feedback inhibition both act through deep-layer Martinotti cells (red and blue stripes). IC, inhibitory cell. **c**, Data fitted with the model by mimicking the pharmacological blocking experiments in L5 and L1 (see Supplementary Information, model description). Inset, model responses scaled to the number of neurons in the population recruitable for Ca^{2+} spikes. **d**, Effects of blocking feedback and feed-forward inhibition, respectively (see text and also Supplementary Fig. 10, which shows the effect of changing the strength of inhibition on the slope).

inhibition is blocked (for example for gabazine to the cortical surface; Fig. 4c). The dendritic population response curves for the pharmacological blocking experiments could be reproduced by removing the corresponding model connectivity to upper and lower layers, respectively (Fig. 4b, c). The model also predicts that blocking the feed-forward drive onto the inhibitory Martinotti cells²⁶ merely shifts the response curve to the left by reducing its threshold (Fig. 4d, light blue), whereas blocking feedback inhibition^{20,21} increases the gain of the response curve and thus modulates the dynamic range of the population calcium response (Fig. 4d, pink; see Supplementary Fig. 11 for further details).

We conclude that the representation of sensory stimuli by cortical output neurons cannot be fully explained by the traditional axosomatic integration approach, but requires active dendrites embedded within highly specialized cortical microcircuitry. Dendritic activity is tightly controlled by interneurons projecting from deep to upper layers (Martinotti cells) whose function was previously unknown. We show here that these neurons dynamically modulate the slope and threshold of the dendritic response function to match the physiologically relevant input range.

METHODS SUMMARY

Female Wistar rats (24–40 d old) were used for these experiments. Multiple dendrites of L5 pyramidal cells were loaded with a Ca^{2+} -sensitive dye, Oregon Green 488 BAPTA-1 AM (OGB-1 AM), by means of bolus injection to L5 (ref. 17). Fibre-optic calcium imaging *in vivo* was performed in the primary somatosensory cortex of awake and urethane-anaesthetized rats as described previously¹⁷ (Fig. 1). Briefly, we used a custom-built microscope attached to a fibre-optic cable (IGN-06/17, 680- μm diameter, Sumitomo Electric Industries). A GRIN lens, right-angled prism (500 \times 500 μm ; GrinTech) assembly was attached to the end of the fibre and the prism inserted into the hindlimb area of the somatosensory cortex (determined beforehand with intrinsic imaging). Sensory responses were evoked by brief air puffs (50-ms duration) delivered to the contralateral hindlimb or a single short electrical microstimulation pulse (0.1-ms duration, 5–200 V) through a surface electrode. All stimuli were below the threshold for muscle responses in the hindlimb. *In vitro* patch-clamp recordings from L5 pyramidal cells were made in parasagittal slices prepared with standard techniques²⁵. Statistical analysis was performed with paired *t*-tests unless otherwise noted; asterisks denote $P < 0.05$.

Full Methods and any associated references are available in the online version of the paper at www.nature.com/nature.

Received 31 July; accepted 18 November 2008.

Published online 18 January 2009.

- London, M. & Häusser, M. Dendritic computation. *Annu. Rev. Neurosci.* **28**, 503–532 (2005).
- Llinás, R. R. The intrinsic electrophysiological properties of mammalian neurons: insights into central nervous system function. *Science* **242**, 1654–1664 (1988).
- Johnston, D., Magee, J. C., Colbert, C. M. & Christie, B. R. Active properties of neuronal dendrites. *Annu. Rev. Neurosci.* **19**, 165–186 (1996).
- Destexhe, A., Mainen, Z. F. & Sejnowski, T. J. Synthesis of models for excitable membranes, synaptic transmission and neuromodulation using a common kinetic formalism. *J. Comput. Neurosci.* **1**, 195–230 (1994).
- Larkum, M. E., Senn, W. & Lüscher, H.-R. Top-down dendritic input increases the gain of layer 5 pyramidal neurons. *Cereb. Cortex* **14**, 1059–1070 (2004).
- Schiller, J., Schiller, Y., Stuart, G. & Sakmann, B. Calcium action potentials restricted to distal apical dendrites of rat neocortical pyramidal neurons. *J. Physiol. (Lond.)* **505**, 605–616 (1997).
- Kim, H. G. & Connors, B. W. Apical dendrites of the neocortex: correlation between sodium- and calcium-dependent spiking and pyramidal cell morphology. *J. Neurosci.* **13**, 5301–5311 (1993).
- Larkum, M. E. & Zhu, J. J. Signaling of layer 1 and whisker-evoked Ca^{2+} and Na^{+} action potentials in distal and terminal dendrites of rat neocortical pyramidal neurons *in vitro* and *in vivo*. *J. Neurosci.* **22**, 6991–7005 (2002).
- Williams, S. R. & Stuart, G. J. Mechanisms and consequences of action potential burst firing in rat neocortical pyramidal neurons. *J. Physiol. (Lond.)* **521**, 467–482 (1999).
- White, E. L. & Hersch, S. M. A quantitative study of thalamocortical and other synapses involving the apical dendrites of corticothalamic projection cells in mouse Sml cortex. *J. Neurocytol.* **11**, 137–157 (1982).
- Hersch, S. M. & White, E. L. Thalamocortical synapses with corticothalamic projection neurons in mouse Sml cortex: electron microscopic demonstration of a monosynaptic feedback loop. *Neurosci. Lett.* **24**, 207–210 (1981).
- Zhu, Y. & Zhu, J. J. Rapid arrival and integration of ascending sensory information in layer 1 nonpyramidal neurons and tuft dendrites of layer 5 pyramidal neurons of the neocortex. *J. Neurosci.* **24**, 1272–1279 (2004).
- Oda, S. *et al.* Thalamocortical projection from the ventral posteromedial nucleus sends its collaterals to layer I of the primary somatosensory cortex in rat. *Neurosci. Lett.* **367**, 394–398 (2004).
- Budd, J. M. L. Extrastriate feedback to primary visual cortex in primates: a quantitative analysis of connectivity. *Proc. R. Soc. Lond. B* **265**, 1037–1044 (1998).
- Cauller, L. J. & Connors, B. W. Synaptic physiology of horizontal afferents to layer-I in slices of rat SI neocortex. *J. Neurosci.* **14**, 751–762 (1994).
- Elhanany, E. & White, E. L. Intrinsic circuitry: synapses involving the local axon collaterals of corticothalamic projection neurons in the mouse primary somatosensory cortex. *J. Comp. Neurol.* **291**, 43–54 (1990).
- Murayama, M., Pérez-García, E., Lüscher, H. R. & Larkum, M. E. Fiberoptic system for recording dendritic calcium signals in layer 5 neocortical pyramidal cells in freely moving rats. *J. Neurophysiol.* **98**, 1791–1805 (2007).
- Kerr, J. N., Greenberg, D. & Helmchen, F. Imaging input and output of neocortical networks *in vivo*. *Proc. Natl Acad. Sci. USA* **102**, 14063–14068 (2005).
- Cauller, L. Layer I of primary sensory neocortex: Where top-down converges upon bottom-up. *Behav. Brain Res.* **71**, 163–170 (1995).
- Silberberg, G. & Markram, H. Disynaptic inhibition between neocortical pyramidal cells mediated by Martinotti cells. *Neuron* **53**, 735–746 (2007).
- Kapfer, C., Glickfeld, L. L., Atallah, B. V. & Scanziani, M. Supralinear increase of recurrent inhibition during sparse activity in the somatosensory cortex. *Nature Neurosci.* **10**, 743–753 (2007).

22. Larkum, M. E., Kaiser, K. M. & Sakmann, B. Calcium electrogenesis in distal apical dendrites of layer 5 pyramidal cells at a critical frequency of back-propagating action potentials. *Proc. Natl Acad. Sci. USA* **96**, 14600–14604 (1999).
23. Helmchen, F., Svoboda, K., Denk, W. & Tank, D. W. *In vivo* dendritic calcium dynamics in deep-layer cortical pyramidal neurons. *Nature Neurosci.* **2**, 989–996 (1999).
24. Larkum, M. E., Zhu, J. J. & Sakmann, B. A new cellular mechanism for coupling inputs arriving at different cortical layers. *Nature* **398**, 338–341 (1999).
25. Pérez-Garci, E., Gassmann, M., Bettler, B. & Larkum, M. E. The GABAB1b isoform mediates long-lasting inhibition of dendritic Ca²⁺ spikes in layer 5 somatosensory pyramidal neurons. *Neuron* **50**, 603–616 (2006).
26. Tan, Z., Hu, H., Huang, Z. J. & Agmon, A. Robust but delayed thalamocortical activation of dendritic-targeting inhibitory interneurons. *Proc. Natl Acad. Sci. USA* **105**, 2187–2192 (2008).

Supplementary Information is linked to the online version of the paper at www.nature.com/nature.

Acknowledgements We thank K. Martin, H.-R. Lüscher and Y. Kudo for their comments on the manuscript, O. Gschwend for support in the laboratory, D. Morris for software development, D. Limoges and J. Burkhalter for their expert technical support and K. Fischer for Neurolucida reconstructions of the biocytin-filled neurons. We also thank Sumitomo Electric Industries for their generous donation of the optical fibre. This work was supported by the Swiss National Science Foundation (grant no. PPOOA-102721/1).

Author Contributions M.M. and M.E.L. designed the study. M.M. performed the periscope experiments *in vivo*, E.P.-G. performed the *in vitro* experiments, and T.N. and M.M. performed the *in vivo* two-photon experiments. W.S. and T.B. made the model and the supplementary model description. M.M. and M.E.L. prepared the manuscript.

Author Information Reprints and permissions information is available at www.nature.com/reprints. Correspondence and requests for materials should be addressed to M.E.L. (larkum@pyl.unibe.ch).

METHODS

The following methods have already been mostly described in ref. 17.

Animals and surgery. Female Wistar rats (P24–P40) were used in these experiments. Urethane (intraperitoneal, 1.5 g kg^{-1}) was used for experiments under anaesthesia. The head was fixed in a stereotaxic instrument (Model SR-5R, Narishige) and body temperature maintained at 36 to 37°C . A craniotomy above the primary somatosensory cortex ($3 \times 4.4 \text{ mm}$ square), centred at 1.5 mm posterior to bregma and 2.2 mm from midline in the right hemisphere, was performed and the dura mater surgically removed immediately before Ca^{2+} recording (see below). For awake experiments, the scalp was removed under general anaesthesia (isoflurane, Baxter) and a local anaesthetic (lidocaine; Sigma-Aldrich) was applied to the wound. Following surgery, an analgesic was administered (buprenorphine (twice per day), Essex Chemie) and local anaesthetic applied to the scalp. On the day of the experiment, a craniotomy was performed, a Ca^{2+} -sensitive dye was injected into L5 (see below) and a metal post was fixed to the skull with dental cement. After anaesthesia, the animals were retrained in a holder (Clam005, Kent Scientific).

In vivo loading of Ca^{2+} -sensitive dye. Oregon Green 488 BAPTA-1 (OGB-1) AM ($50 \mu\text{g}$; Molecular Probes) was mixed with $5 \mu\text{l}$ of pluronic acid (Pluronic F-127, 20% solution in dimethylsulphoxide; Molecular Probes) for 15 min. The solution was then diluted in $28 \mu\text{l}$ of HEPES-buffered solution (125 mM NaCl , 2.5 mM KCl , 10 mM HEPES) and mixed for a further 15 min. The OGB-1 AM solution was loaded into a glass pipette (tip diameter, $5\text{--}20 \mu\text{m}$) and pressure-injected into L5 (pressure, $10\text{--}25 \text{ kPa}$) for 1 min. The pipette was withdrawn and the area of the craniotomy was then submerged with rat ringer (135 mM NaCl , 5.4 mM KCl , 1.8 mM CaCl_2 , 1 mM MgCl_2 , 5 mM HEPES) for 2 h.

In vivo Ca^{2+} recording (periscope). A 100-W mercury lamp (U-LH100HG, Olympus) or a blue light-emitting-diode (LED, IBF+LS30W-3W-Slim-RX, Imac) was used as a light source. An excitation filter, a dichroic mirror, and an emission filter (as a filter set 31001, Chroma Technology) were used for epifluorescence Ca^{2+} recordings. A $\times 10$ objective (0.45 numerical aperture, Model E58-372, Edmund Optics) was used for illuminating and imaging a fibre bundle (see below). A cooled charge-coupled-device (CCD) camera (MicroMax, Roper Scientific) was used for collecting fluorescence.

A fibre bundle (IGN-06/17, Sumitomo Electric Industries) consisting of 17,000 fibre elements was used as a combined illuminating–recording fibre. The end face of the bundle was fitted with a prism-lens assembly that consisted of a right-angled prism ($0.5 \times 0.5 \times 0.5 \text{ mm}$; GrinTech) attached to a GRIN lens (diameter, 0.5 mm ; 0.5 numerical aperture; GrinTech). The working distance was nominally $100 \mu\text{m}$ and the magnification was $\times 0.73$, resulting in a field of view of $685\text{-}\mu\text{m}$ diameter.

Sensory responses were evoked by a brief air puff (50-ms duration) delivered to the contralateral hindlimb or a single short electrical stimulation (0.1-ms duration, $5\text{--}200 \text{ V}$). Fluorescence changes were sampled at 100 Hz . Data were acquired on a personal computer using WinView software (Roper Scientific). Regions of interest were chosen offline for measuring fluorescence changes (see data analysis section). Gabazine and CGP52432 were bought from Biotrend Chemicals, tetrodotoxin (TTX) from Tocris Cookson and cadmium chloride from Fluka.

In vivo Ca^{2+} recording (two-photon). Two-photon excitation fluorescence microscopy was either performed with a femtosecond infrared laser ($\lambda = 800\text{--}810 \text{ nm}$, 100 fs ; Tsunami pumped by a Millennia VIII or Mai-Tai HP, Spectra-Physics) coupled to a laser scanning microscope (TCS SP2RS, Leica) equipped with a $\times 40$ water immersion objective (HCX APO w40x, UVI, numerical aperture 0.8) or a custom-built two-photon microscope equipped with a $\times 20$ water immersion objective (numerical aperture 0.95; Olympus). Excitation infrared-laser light and fluorescence-emission light were separated at 670 nm (excitation filter 670DCXXR, AHF Analysentechnik) and the infrared light was blocked in the detection pathway with an infrared-block filter (E700SP, AHF Analysentechnik). Fluorescence was detected using epifluorescence non-descanned detection. Calcium transients were recorded in line-scan mode at 500 Hz from identified L5 tuft dendrites.

In vitro experiments. Animals were anaesthetized with a mixture of $95\% \text{ CO}_2/5\% \text{ O}_2$ before decapitation. The brain was then rapidly transferred to ice-cold, oxygenated artificial cerebrospinal fluid (ACSF) containing 125 mM NaCl , 25 mM NaHCO_3 , 2.5 mM KCl , $1.25 \text{ mM NaH}_2\text{PO}_4$, 1 mM MgCl_2 , 25 mM glucose and 2 mM CaCl_2 ($\text{pH } 7.4$). Parasagittal slices of the primary somatosensory cortex ($300\text{-}\mu\text{m}$ thick) were cut with a vibrating microslicer on a block angled at 15° to the horizontal and maintained at 37°C in the preceding solution for $15\text{--}120 \text{ min}$ before use.

Ca^{2+} imaging and somatic whole-cell patch recordings of L5 neurons were obtained with Nikon Eclipse E600FN microscopes (Nikon). Ca^{2+} imaging was performed using a CCD camera (CoolSNAP, Roper Scientific). The fluorescence was observed using standard epifluorescence filter sets for fluorescein (excitation at 480 nm ; used for OGB-1) and Texas Red (Alexa 594; Molecular Probes) fluorescence (Chroma Technology). Fluorescence intensities were sampled at $30\text{--}40 \text{ Hz}$. Pipettes ($4\text{--}6 \text{ M}\Omega$) for the whole-cell patch-clamp recordings were filled with an intracellular solution containing $135 \text{ mM K-gluconate}$, 7 mM KCl , 10 mM HEPES , $10 \text{ mM Na}_2\text{-phosphocreatine}$, 4 mM Mg-ATP , 0.3 mM GTP , 10 mM Alexa 594 and 0.2% biocytin ($\text{pH } 7.2$ with KOH). No correction was made for the junction potential between the bath and pipette solutions. The recordings were made with Multiclamp 700B (Axon Instruments), digitized at 10 kHz with an analogue–digital converter (ITC-16 Instrutech) and acquired on a personal computer using Igor software (WaveMetrics). Dendritic Ca^{2+} spikes were evoked with EPSP-shaped current waveforms injected through a dendritic pipette: double exponential, $f_{(t)} = (1 - e^{-t/\tau_1})e^{-t/\tau_2}$, where $\tau_1 = 4 \text{ ms}$ and $\tau_2 = 10 \text{ ms}$; time to peak, 5 ms . Slices were perfused continuously with the ACSF at $33\text{--}35^\circ\text{C}$ throughout the experiments.

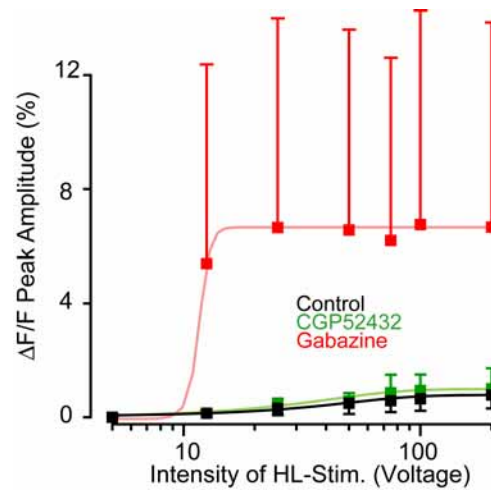
Data analysis. The fluorescence signals *in vivo* were quantified by measuring the mean pixel value of a manually selected (offline) ROI for each frame of the image stack using Igor software. Ca^{2+} changes were expressed as $\Delta F/F = F_t/F_0$, where F_t was the average fluorescence intensity within the ROI at time t during the imaging experiment and F_0 was the mean value of fluorescence intensity before stimulation. For *in vitro* experiments, Ca^{2+} changes were expressed as $\Delta F/F = (F_t - F_0)/(F_0 - F_B)$, where F_B is the background fluorescence measured from a region away from the recorded area.

Model. The full model comprises microcircuitry with two types of inhibitory neuron and a population of N two-compartment pyramidal neurons displaying all-or-none dendritic calcium events (0 or c). The mathematical analysis of the microcircuitry leads to a compact description of the population calcium response, $C(S)$, as a function of the stimulus strength, S , and the feed-forward and feedback connection strengths $\beta^{\text{ff}} = \text{FF}_e - \text{FF}_i$ and $\beta^{\text{fb}} = \text{FB}_e - \text{FB}_i$, respectively. We fit the distribution of the calcium activation thresholds (mean, θ_0 ; standard deviation, σ) such that the steep response curve for TTX (modelled by $\beta^{\text{fb}} = 0$) is reproduced. The population calcium response can be approximated by the sigmoidal function

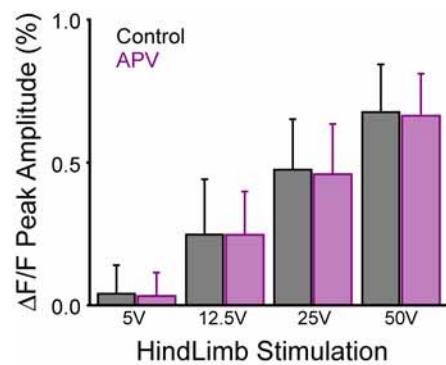
$$C(S) \approx \frac{Nc}{1 + \exp(-\gamma(\beta^{\text{ff}} \log S - (\theta_0 + \theta_1))/\sigma)}$$

with gain factor $\gamma = (1 - \beta^{\text{fb}}c/4\sigma)^{-1}$ and threshold shift $\theta_1 = -\beta^{\text{fb}}c/2$; see Supplementary Information, model description. The pharmacological blocking experiments are described by assuming that the corresponding model connections are removed (Fig. 4b, c), and this changes the values of β^{ff} and β^{fb} . Roughly speaking, these experiments lead to an increase in β^{fb} (CNQX, TTX, gabazine to L1) with a corresponding gain increase, and to a reduction in β^{ff} (gabazine to L5) with a corresponding rightwards shift of the $C(S)$ curve. Analogously, blocking the feed-forward excitation of the (inhibitory) model Martinotti cells increases β^{ff} and leads to a leftwards shift of $C(S)$, whereas blocking the Martinotti cell output increases β^{fb} and leads to a gain increase (blue and pink curves in Fig. 4d). The number of pyramidal neurons, N , that can be recruited to contribute to the population calcium signal is a nonlinearly increasing function of the dendritic feedback strength β^{fb} and a linearly increasing function of the gain factor γ (see Supplementary Information, model description).

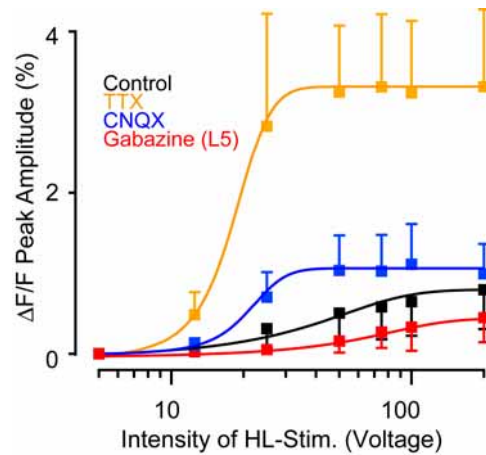
SUPPLEMENTARY INFORMATION



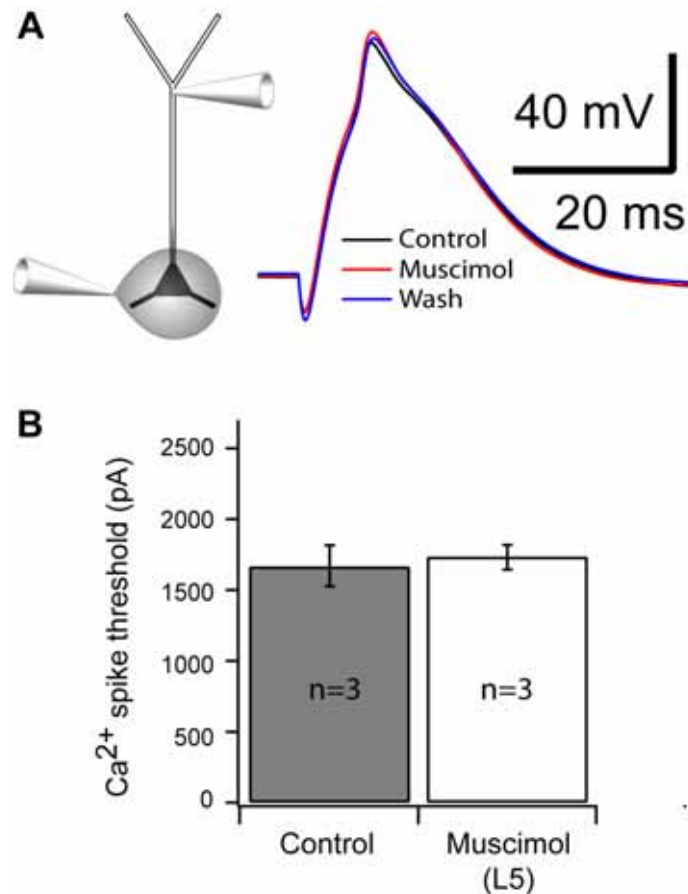
Supplementary Figure 1. Non-normalized data of $\Delta F/F$ peak amplitude of dendritic Ca^{2+} signals evoked by hind limb stimulation. CGP52432 (green, $n = 6$) and gabazine (red, $n = 6$) were applied to cortical surface (see text).



Supplementary Figure 2. Hindlimb stimulation evoked $\Delta F/F$ peak amplitude of dendritic Ca^{2+} signals ($n = 6$) before and after application of APV (100 μM), an antagonist of NMDA receptors, to cortical surface. $P > 0.1$.

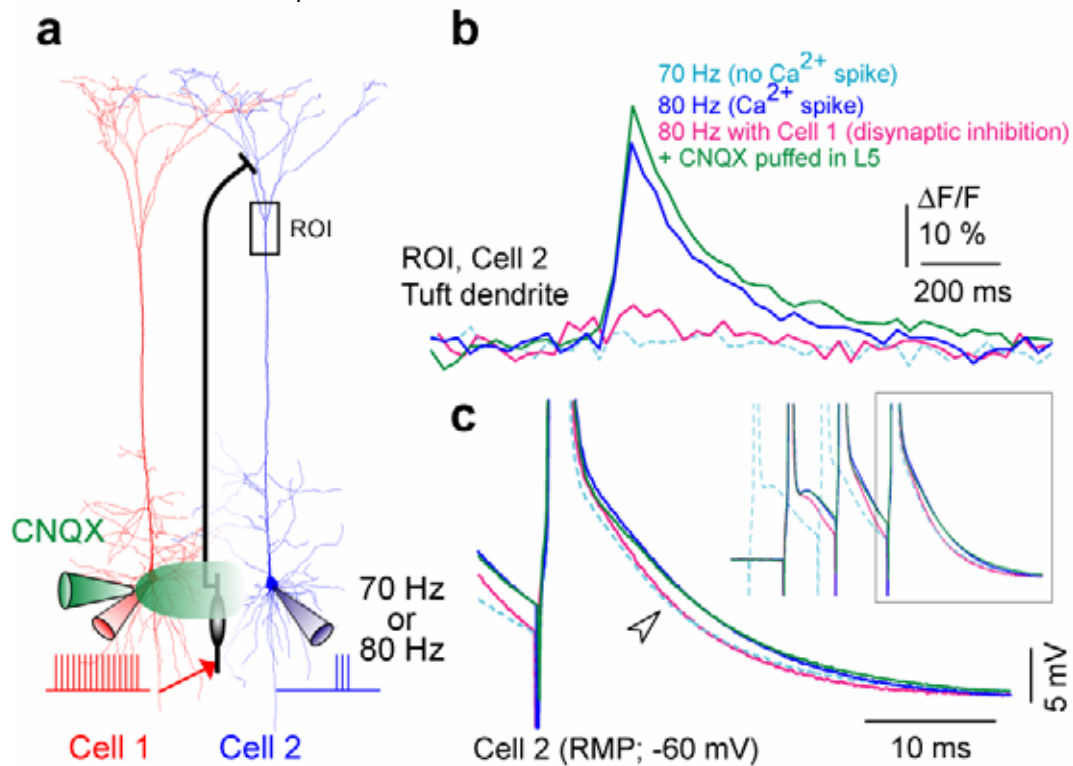


Supplementary Figure 3. Non-normalized data of $\Delta F/F$ peak amplitude of dendritic Ca^{2+} signals with TTX (orange, $n = 5$), CNQX (blue, $n = 5$) and gabazine (red, $n = 5$). The drugs were applied into L5 separately (see text).



Supplementary Figure 4. Inhibition of Na^+ and activation of GABA_A receptor channels at the peri-somatic area, does not influence the generation of dendritic Ca^{2+} spikes. **a**, Left, Schematic diagram of experiment. A dendritic patch recording at $>500 \mu\text{m}$ from the cell body was used to generate and record a Ca^{2+} spike. TTX ($3 \mu\text{M}$) was local applied to the peri-somatic region. Right, Dendritically recorded traces showing that suprathreshold Ca^{2+} spikes (red) could be generated with current injection above 2300 pA in an all-or-none fashion. **b**, Muscimol did not change the threshold for the generation of dendritic Ca^{2+} spikes with dendritic current injection ($n = 3$; $P = 0.42$). Local application

of muscimol (20 μ M) to L5 (analogous to the *in vivo* experiments of Fig. 2) did not change the threshold for dendritic Ca^{2+} spikes using dendritic current injection (1.67 ± 0.25 nA vs. 1.73 ± 0.15 nA, $P = 0.42$, $n = 3$, data not shown), indicating that somatic inhibition has very little effect on the generation of dendritic Ca^{2+} spikes.



Supplementary Figure 5. Disynaptic inhibition blocks dendritic Ca^{2+} activity induced by high-frequency back-propagating APs. **a**, Experimental diagram showing reconstructed L5 pyramidal neurons and recording sites (same experiment as in Fig. 3 e & f). **b**, We have previously shown that there is a critical frequency of back-propagating APs which generate dendritic Ca^{2+} spikes²³. Here, trains of somatic action potentials at a sub-critical frequency (70 Hz) did not evoke a dendritic calcium transient in the apical tuft initiation zone (dashed cyan), whereas an increase of 10 Hz in the frequency of back-propagating APs (the critical frequency, 80 Hz) evoked substantial, all-or-none Ca^{2+} transient in the same region (dark blue) with a accompanying increase in somatic membrane potential directly after the last AP in the train (see part c). Simultaneous disynaptic inhibition abolished the dendritic transient (pink) which was recovered after application of 20 μ M CNQX to L5 (green). **c**, The afterdepolarizing potential (ADP) measured after the last AP at the soma reflects the changes in Ca^{2+} influx into the dendritic Ca^{2+} spike initiation zone. Magnified view of the ADPs (arrowhead). An increase in the amplitude of the ADP from 70 to 80 Hz was indicative of a dendritic Ca^{2+} spike. Disynaptic inhibition reversed the amplitude of the ADPs to sub-critical frequency values (pink; $P < 0.05$, $n = 8$). The amplitude of the ADPs recovered after perisomatic application of CNQX to control values (green).

Supplementary model description

Remarks on the model design

We present a mathematical model which allows us to describe the various pharmacological blocking experiments and to reproduce the corresponding population calcium responses as presented in the main text. A minimal phenomenological model which captures the dependence of the calcium response function from the feedforward and feedback connection strengths consists of a simple feedback circuitry as shown in the Supp. Fig. M3. This simple feedback circuitry is mathematically deduced from the full model (Supp. Figs M1, 2) and describes the calcium signal C in response to a stimulus of strength S .

In the steady state the calcium response function $C(S)$ is a sigmoidal which depends on three effective parameters, the saturation level, the half-activation ('shift'), and the gain. Each of these parameters can be expressed in terms of the feedforward/feedback connection strengths and the calcium spike characteristics (see Eqs 14 – 15). This minimal model captures the differential effects of the feedforward and feedback inhibition on the gain and the shift of the response function (Fig. 4d, main text and Full Methods).

The simple feedback circuitry also allows us to fit the response curves for the various pharmacological blocking experiments. In fact, since each of the five response curves can be characterized by 3 parameters (saturation, shift and gain) it is always possible to fit each by adapting the 3 model parameters, the number of recruitable pyramidal neurons (determining the saturation level), the strength of the feedforward connection (affecting the shift), and the strength of the feedback connection (affecting gain and shift). To reduce the number of free parameters we further constrain the model by considering pyramidal neurons embedded in a microcircuitry with distributed excitatory and inhibitory feedback and feedforward projections. For each pharmacological blocking experiment we then define a set of connections which are deleted from the model microcircuitry to determine the corresponding calcium response curve (see Supp. Fig. M4). Given these sets we tuned 10 parameter values (6 connections strengths and 4 different numbers of recruitable pyramidal neurons) to fit the 5 sigmoidal response curves which by themselves would require a total of 15 values (see Table 1). Hence, the structure of the model circuitry allows us to reduce the 15 degrees of freedom to effectively 10 free parameter choices. The extended model is therefore constrained enough to unravel intrinsic dependencies in the data and to explain them with a reduced set of physiologically interpretable (although not yet measured) parameters.

A second step beyond the simple calcium feedback circuitry consists in introducing a 2-compartment pyramidal cell model with current-to-frequency transfer function extracted from previous data (Larkum et al., 2004). All the parameter values describing the pyramidal neurons are fixed to the values extracted from this previous data. Including these model pyramidal cells represents a genuine extension since it takes the current-frequency feedback circuitry into account which underlies the recruitment of dendritic calcium currents. As a consequence, for instance, the effective feedforward drive of the calcium signal becomes itself dependent on the feedback connection strength. In fact, the feedback contributes to the dendritic current already before it is crossing the calcium spike threshold. Beside these complications, we also consider the voltage interactions between the somatic and dendritic compartments.

The mathematical analysis of the extended model yields a reduction of the full microcircuitry of pyramidal cells and interneurons to the original simple calcium feedback circuitry, but now with parameters being expressed in terms of biophysical quantities (Eqs 15&16). It provides an explicit dependence of the population calcium response curves on each of the pyramidal cell and microcircuitry parameters. The close link between phenomenological observations and the

microscopic parameters allows us to make quantitative predictions for further pharmacological modulations, e.g. of specific connections to or from Martinotti cells (see Supp. Fig. M5).

The model

Pyramidal neurons and microcircuitry. We consider a population of N pyramidal neurons, each with a somatic and dendritic compartment (Fig. M1, M2). The somatic compartments receive a feedforward synaptic current of the form

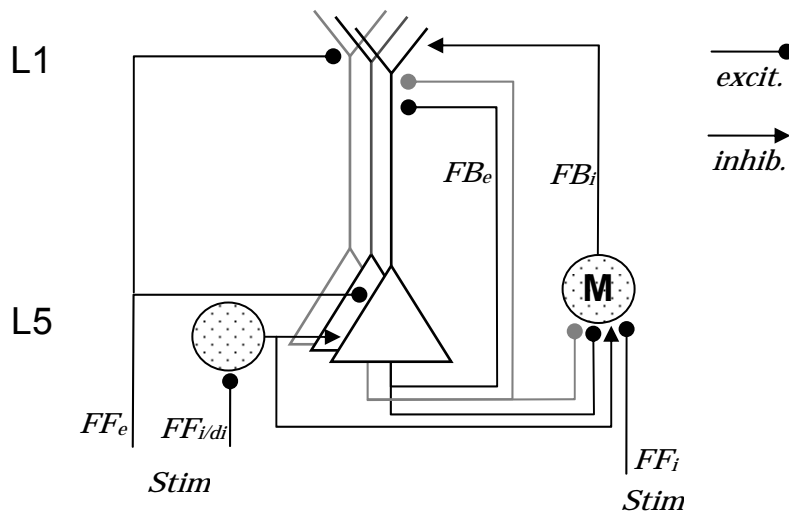
$$I_{syn}^{som}(S) = \alpha^{ffsom} \log S \quad (1)$$

in response to a sensory stimulation of strength S . The factor is composed of an excitatory component and an inhibitory component mediated through an inhibitory neuron $\alpha^{ffsom} = \alpha_{ex}^{ffsom} - \alpha_{inh}^{ffsom}$. The logarithmic dependence on the stimulus strength represents Weber's law and arises from the various saturation mechanisms in the upstream sensory processing. These input currents are assumed to last for a duration of at least 90ms following the electrical hind limb pulse as this time delay corresponds to the observed delay of the calcium fluorescence peak activity.

The total synaptic input to the dendritic compartment, $I_{syn}^{den}(S)$, is composed of feedback input from the pyramidal cell population itself and the feedforward input, both targeting the dendrite either directly or through the Martinotti cells (Fig. M2). To simplify matters we assume that the transfer functions of the Martinotti cells and the second inhibitory neuron in L5 are linear. The total synaptic input targeting the dendritic compartment can be written in the form

$$I_{syn}^{den} = \frac{\alpha^{fbden}}{N} \sum_{i=1}^N f_i^{pyr}(S) + \alpha^{ffden} \log S. \quad (2)$$

where $f_i^{pyr}(S)$ represents the firing rate of the i th pyramidal neuron and the constants are $\alpha^{fbden} = \alpha_{ex}^{fbden} - \alpha_{inh}^{fbden}$ and $\alpha^{ffden} = \alpha_{ex}^{ffden} - \alpha_{inh}^{fbden} (\alpha_{ex}^{ffM} - \alpha_{inh}^{ffM})$, see Fig. M2. Note that the total feedforward input current to the Martinotti cells is $I^{ffM}(S) = (\alpha_{ex}^{ffM} - \alpha_{inh}^{ffM}) \log S$, and that the (inhibitory) feedforward input to the dendrites mediated by the Martinotti cells is $-\alpha_{inh}^{fbden} I^{ffM}(S)$. In turn, the (inhibitory) feedback component from the pyramidal neurons mediated by the same Martinotti cells is $-\alpha_{inh}^{fbden} 1/N \sum f_i^{pyr}(S)$. Adding to this the excitatory feedforward and feedback inputs yields Eq. 2.

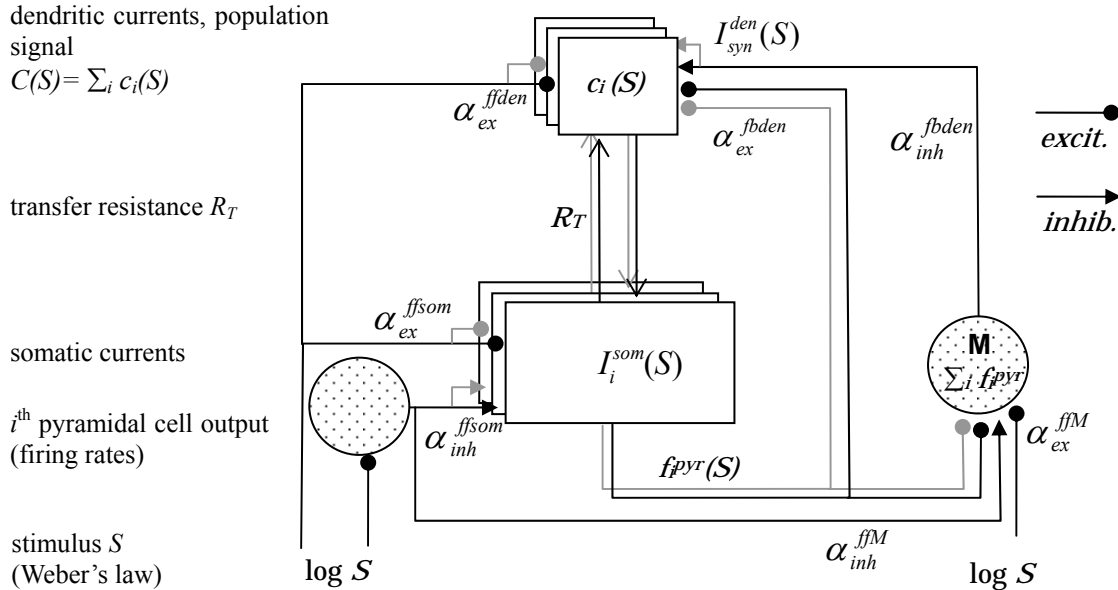


Supplementary Figure M1. Model of the cortical microcircuitry. A population of layer 5 pyramidal neurons driven by the stimulus (*Stim*) through excitatory feedforward connections (FF_e) to both the somatic and dendritic region, and by inhibitory feedforward connections (FF_i) via Martinotti cells (*M*) to the dendritic region. Feedback from the pyramidal neurons is directly exciting the pyramidal cell dendrites (FB_e), or is inhibiting them via Martinotti cells (FB_i). The soma also receives direct inhibition, while the dendrites are disinhibited via inhibition targeting Martinotti cells ($FF_{i/di}$). Feedforward and feedback input to the dendrites differently affect the population calcium response.

Passive pyramidal cell properties. The 2-compartment pyramidal cell model is specified by the somatic and dendritic membrane resistance R_m^{som} and R_m^{den} , respectively, and transfer resistance R_T (Fig. M2). Given the 90ms delay of the peak fluorescence signal with respect to the sensory stimulation, we assume that the somatic and dendritic voltages converged to a steady state. The total synaptically generated current in the dendrite (i.e. the synaptic currents from soma and dendrite without dendritic calcium current) then becomes

$$I_0^{den}(S) = \lambda^{som} I_{syn}^{som} + (1 - \lambda^{den}) I_{syn}^{den}, \quad (3)$$

where $\lambda^{som} = R_m^{som} / (R_m^{som} + R_m^{den} + R_T)$ and $\lambda^{den} = R_m^{den} / (R_m^{som} + R_m^{den} + R_T)$ represent the fractions of currents leaking away from the soma and dendrite, respectively, into the other compartment (for a derivation of Eq. 3 see Endnote 1). Hence, the dendritic compartment shares a fraction λ^{som} of the somatic input, and a fraction $(1 - \lambda^{den})$ of the dendritic input.



Supplementary Figure M2. Model and mathematical quantities. A population of layer 5 pyramidal neurons, each with a somatic compartment receiving feedforward input, and a dendritic compartment receiving feedforward and feedback input via excitatory and inhibitory (Martinotti) neuron. If the total input to the dendrite, $I_0^{den}(S)$, in response to stimulus S exceeds a cell-specific threshold (θ_i), a calcium spike of strength c is elicited. The measured calcium fluorescence signal corresponds to the population calcium signal $C(S) = \sum_i c_i(S)$ summed across the dendrites of all pyramidal neurons $i=1, \dots, N$.

Dendritic calcium spikes. Whenever the total synaptically generated dendritic current $I_0^{den}(S)$ exceeds a cell specific threshold θ_i (with $i=1, \dots, N$) a dendritic calcium spike is triggered. This spike is modeled as a plateau current of constant strength c ¹. The dendritic calcium current in pyramidal cell i is captured by the Heaviside step function

$$c_i(S) = c H(I_0^{den}(S) - \theta_i) = \begin{cases} c & \text{if } I_0^{den}(S) > \theta_i \\ 0 & \text{else} \end{cases}, \quad (4)$$

where $H(x) = 0$ if $x < 0$ and 1 else. We assume that the calcium thresholds θ_i of the i pyramidal neurons are distributed (Gaussian-like) around some mean θ_0 with standard deviation σ .

The population calcium signal in response to stimulus S is

$$C(S) = \sum_{i=1}^N c_i(S), \quad (5)$$

and this corresponds to the quantity which is experimentally measured via calcium fluorescence.

Pyramidal cell firing rate. The dendritically generated current $I_{syn}^{den}(S) + c_i(S)$ electrotonically propagates to the soma where it adds up with the synaptic current $I^{ff}(S)$ targeting the soma. The total steady state current in the soma generated by the different synaptic inputs and the dendritic calcium

¹ Note: the data cannot distinguish between this and the case that dendritic spikes give variable amplitudes. In the 2nd case, the value c can be interpreted as the average Ca²⁺ entry accompanying a dendritic spike.

spike is calculated to be

$$I_i^{som}(S) = \lambda^{den} \left(I_{syn}^{den}(S) + c_i(S) \right) + (1 - \lambda^{som}) I_{syn}^{som}(S). \quad (6)$$

Next we assume that the somatic currents are transformed into asynchronous output firing rates of the pyramidal neurons according to the threshold linear transfer function

$$f_i^{pyr}(S) = g [I_i^{som}(S) - \Theta]^+, \quad (7)$$

where $g > 0$ is the gain of the f - I curve, Θ is the current threshold for generating somatic action potentials, and $[x]^+ = x$ if $x > 0$ and 0 else.

Model analysis

To calculate the population calcium signal $C(S)$ we assume that the stimulation strengths is strong enough to fire the pyramidal neurons by the feedforward input alone. As a consequence, the somatic currents are always in the linear regime of the current-to-frequency transfer function. In this case the feedback circuitry presented in Fig. M2 can be explicitly solved for $C(S)$.

Distribution of dendritic calcium spike thresholds. To calculate $C(S)$ we further consider a continuous distribution of the dendritic calcium spike thresholds $\theta = \theta_i$. We consider a bell-shaped normalized threshold density $\rho\theta$ with mean θ and exponential decay on both sides according to

$$\rho(\theta) = \frac{1}{\sigma} \cdot \frac{1}{1 + e^{(\theta - \theta_0)/\sigma}} \cdot \frac{1}{1 + e^{-(\theta - \theta_0)/\sigma}}, \quad (8)$$

where σ is the width of the exponential decay (Suppl. Fig. M5b, green curve). A Gaussian threshold distribution instead of distribution (8) would lead to qualitatively similar results but the density (8) is mathematically convenient (as it is the derivative of a Boltzmann function). Instead of the index i , the pyramidal neurons are now parameterized by their characterizing calcium threshold θ . The dendritic calcium signal of pyramidal cell θ s then

$$c_\theta(S) = c \text{H}(I_0^{den}(S) - \theta) \quad (4')$$

instead of (4).

The population calcium signal. To simplify the mathematical treatment we replace the sum defining the population signal (Eq. 5) by an integral across calcium responses parameterized by the calcium threshold. Assuming a density $\rho\theta$ of calcium thresholds, the dendritic calcium signal of the whole population becomes,

$$C(S) = N \int_{-\infty}^{\infty} \rho(\theta) \cdot c_\theta(S) d\theta = N \int_{-\infty}^{\infty} \rho(\theta) \cdot c \cdot \text{H}(I_0^{den}(S) - \theta) d\theta = \frac{Nc}{1 + e^{-(I_0^{den}(S) - \theta_0)/\sigma}}. \quad (9)$$

For the calculation of this integral we refer to Endnote 2. Hence, the population response of the binary calcium spikes is a sigmoidal function in $I_0^{den}(S)$, with a gain $1/\sigma$ being the inverse width of the calcium threshold distribution $\rho\theta$: the wider the threshold distribution, the shallower the population response function. For strong stimulations, $I_0^{den}(S)$ becomes large and each neuron of the population elicits a dendritic calcium spike, yielding the maximal response $C(S) = Nc$.

Deducing the calcium recurrence relation. The formula for the population calcium signal $C(S)$ implicitly represents a recurrence relation as $C(S)$ also determines the dendritic current $I_0^{den}(S)$ occurring in (9). To address this recurrence relation we rewrite the synaptic current in the dendrite, Eq. 2, as

$$I_{syn}^{den}(S) = \alpha^{fden} \int_{-\infty}^{\infty} \rho(\theta) f_\theta^{pyr}(S) d\theta + \alpha^{ffden} \log S, \quad (10)$$

where we again replaced the index i by θ , and the normalized sum $1/N \sum f_i^{pyr}$ by the integral of f_θ^{pyr} , weighted by the normalized threshold density $\rho(\theta)$.

Next we use the assumption that the sensory stimulations always drive the pyramidal neurons. We can then write the pyramidal cell firing rates (7) in the form

$$f_{\theta}^{pyr} = g\left(\lambda^{den}(I_{syn}^{den} + c_{\theta}) + (1 - \lambda^{som})I_{syn}^{som} - \Theta\right), \quad (11)$$

where we substituted the somatic current $I_{\theta}^{som} = \lambda^{den}(I_{syn}^{den} + c_{\theta}) + (1 - \lambda^{som})I_{syn}^{som}$ given by Eq. 6 and where we dropped the dependency on S . Plugging this into the above integral (10), and calculating the integral using (9) and the fact that the integral over $\rho(\theta)$ is normalized to 1, yields

$$I_{syn}^{den} = \alpha^{fbden} g\left(\lambda^{den}(I_{syn}^{den} + C/N) + (1 - \lambda^{som})I_{syn}^{som} - \Theta\right) + \alpha^{ffden} \log S.$$

We can directly solve this recurrence relation for I_{syn}^{den} and get

$$I_{syn}^{den} = b^{fb}\left(\lambda^{den}C/N + (1 - \lambda^{som})I_{syn}^{som} - \Theta\right) + b^{ff} \log S \quad (12)$$

$$\text{with } b^{fb} = \frac{\alpha^{fbden} g}{1 - \alpha^{fbden} g \lambda^{den}} \text{ and } b^{ff} = \frac{\alpha^{ffden}}{1 - \alpha^{fbden} g \lambda^{den}}.$$

We now substitute I_{syn}^{som} and I_{syn}^{den} given by Eqs 1 and 12 in the expression for the dendritic current, Eq. 3, and get

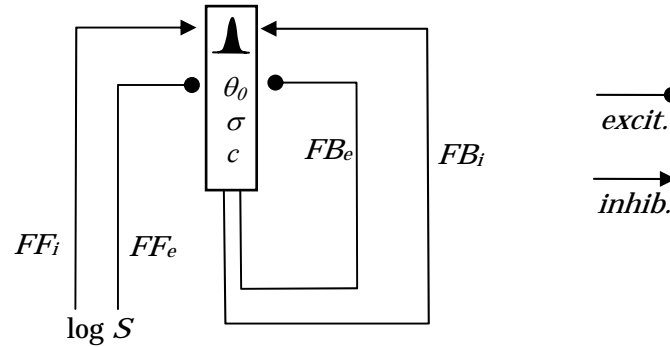
$$I_0^{den} = \beta^{ff} \log S + \beta^{fb}\left(C/N - \Theta / \lambda^{den}\right), \quad (13)$$

$$\text{with } \beta^{ff} = \lambda^{som} \alpha^{ffsom} + (1 - \lambda^{den})\left((1 - \lambda^{som})\alpha^{ffsom} b^{fb} + b^{ff}\right)$$

$$\text{and } \beta^{fb} = (1 - \lambda^{den})\lambda^{den} b^{fb} = (1 - \lambda^{den}) \frac{\alpha^{fbden} g \lambda^{den}}{1 - \alpha^{fbden} g \lambda^{den}}.$$

This expression for I_0^{den} only contains the feedforward stimulus, $\log S$, and the calcium population signal C (recall the definition of λ^{som} and λ^{den} below Eq. 3). Plugging (13) into (9) therefore yields a recurrence relation for $C(S)$,

$$C(S) = \frac{Nc}{1 + e^{-(\beta^{ff} \log S + \beta^{fb}(C(S)/N - \Theta / \lambda^{den}) - \theta_0) / \sigma}}. \quad (14)$$



Supplementary Figure M3. Analytically reduced model. The whole microcircuitry is specified by the effective strength of the feedforward ($\beta^f = FF_e - FF_i$) and the feedback ($\beta^b = FB_e - FB_i$) connections, each composed of an excitatory and inhibitory component. The calcium spike thresholds of the N dendrites are assumed to be Gaussian distributed around θ_0 with standard deviation σ , and each calcium spike produces the signal c . The population calcium signal C as a function of the stimulus strength S is the sigmoidal function $C(S) = Nc / (1 + \exp(-\gamma(\beta^f \log S - (\theta_0 + \theta_1)) / \sigma))$, with $\gamma = (1 - \beta^b c / (4\sigma))^{-1}$ and $\theta_1 = -\beta^b c / 2$ (assuming that the action potential thresholds Θ of the pyramidal neurons are zero). We conclude that increasing the feedback connection strength β^b increases the gain γ , while increasing the feedforward connection strength β^f mainly leads to a threshold decrease θ_1 (and also to a stretching the $\log S$ axis which, for large θ_0 , becomes negligible, however).

Solving the calcium recurrence relation. The recurrent Eq. 14 has only one solution in $C(S)$, provided that β^b is not too large (and in particular if $\beta^b < 0$ for the case that feedback inhibition dominates feedback excitation, $\alpha^{fden} = \alpha_{ex}^{fden} - \alpha_{inh}^{fden} < 0$). Tracing this unique solution for varying S yields a sigmoidal-like function of $\log S$. To study the parameter dependency of this function we approximate it by a pure sigmoidal (i.e. a Boltzmann function) and make the ansatz

$$C(S) \approx \frac{Nc}{1 + e^{-\gamma(\beta^f \log S - (\theta_0 + \theta_1)) / \sigma}} \quad (15)$$

with some additional gain factor γ and some additional shift θ_1 . After some reasoning (see Endnote 3) one finds for the two additional parameters

$$\gamma = \frac{1}{1 - \beta^b c / (4\sigma)} \quad \text{and} \quad \theta_1 = \beta^b \left(\Theta / \lambda^{den} - c / 2 \right), \quad (16)$$

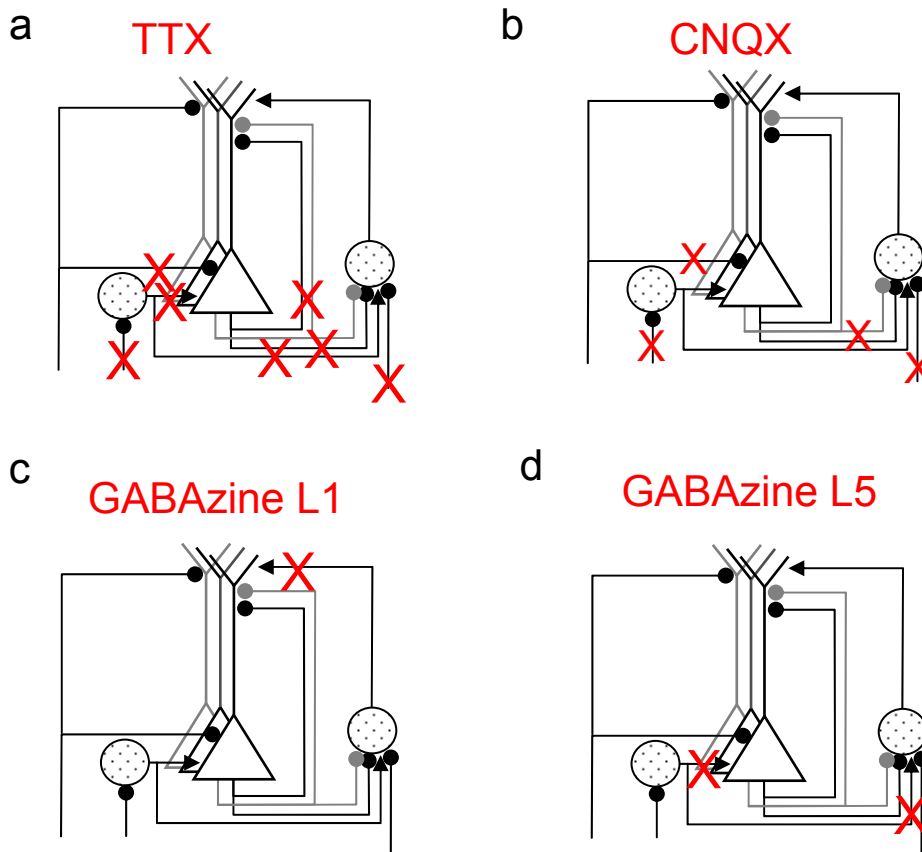
with β^b defined in (13) and λ^{den} defined in (3). Recall that the parameters θ and σ are characterizing the calcium threshold density (8), while c is the strength of the dendritic calcium signal and Θ is the threshold for the somatic action potential.

Increasing the feedback strength α^{fden} increases the gain of the calcium response function (because β^b in the expression of γ is increased) and shifts the midpoint to the left (because increasing β^b makes θ_1 more negative, provided that the calcium signal, after its propagation to the soma, exceeds twice the action potential threshold, $c\lambda^{den}/2 > \Theta$), see Suppl. Fig. M5. Interestingly, the feedback strength α^{fden} can itself be positive and the population activity is still finite, provided that the additional slope factor γ remains itself finite. This is the case for $\beta^b < 4\sigma/c$.

The analytically reduced model

The mathematical analysis reduced the microcircuitry with the 2-compartmental pyramidal neurons (Suppl. Fig. M1, 2) to a simple feedback circuitry for the population calcium signal $C(S)$ (Suppl. Fig.

M3). According the Eq. 14 this feedback circuitry is characterized by the effective feedforward and feedback connection strengths, $\beta^f = FF_e + FF_i$ and $\beta^b = FB_e + FB_i$, the number of pyramidal neurons (N), the strength of a unit calcium spike (c), the distribution of the calcium spike thresholds (θ_0, σ), and the effective action potential threshold normalized by the dendritic leak factor ($\tilde{\theta}^{\lambda^{den}}$). This feedback circuitry for $C(S)$ can be approximated by the Boltzmann function (Eq. 15) with parameter values given in Eq. 16 (cf. Supp. Fig. M5).

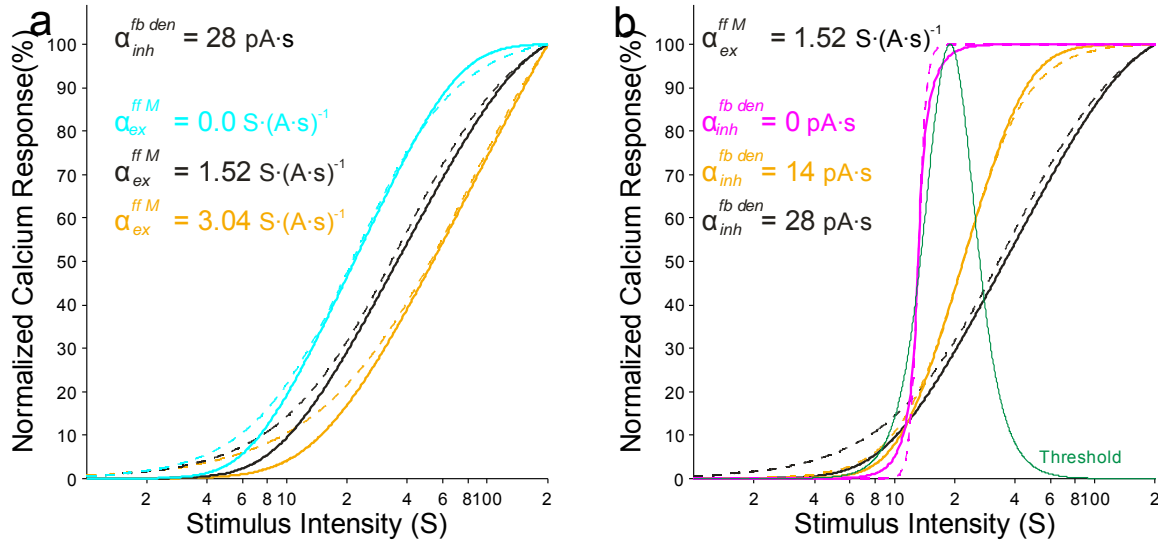


Supplementary Figure M4. Modeling the blocking experiments, red crosses indicate total block, green crosses indicate partial block. **a**, Blocking of action potentials in L5 by local, deep layer application of TTX, **b** competitive partial blocking of excitatory AMPA receptors in L5 by deep layer application of CNQX, **c**, blocking of $GABA_A$ receptors in L1 by surface application of GABAazine, and **d**, blocking of $GABA_A$ receptors in L5 by deep layer application of GABAazine. The crossed synaptic connection strengths are set to 0 in the model. Based on the analytical reduction, the canceling of these specific connections translate into corresponding modifications of the parameters $FF_{e/i}$ and $FB_{e/i}$ characterizing the overall feedforward and feedback connection strengths (see Figs. M1, M3 and Table 1, 2).

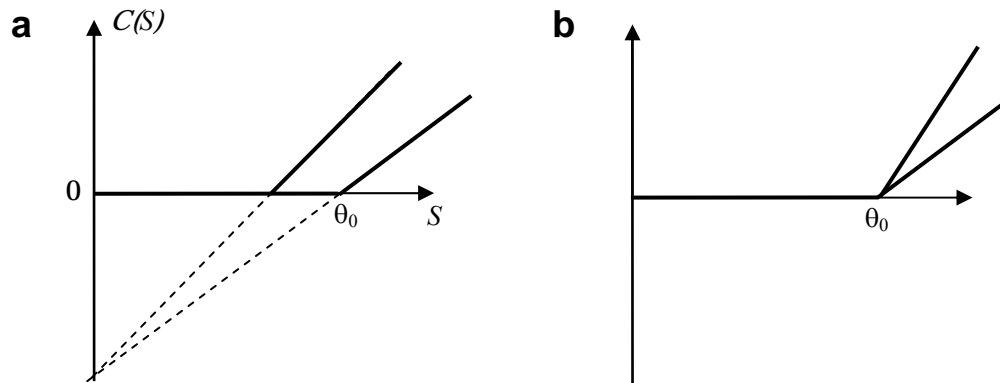
Simulation results

The differential effects of pharmacologically modulating the feedforward and feedback connection strengths is revealed by varying the parameters $\alpha^{f^{den}}$ and $\alpha^{b^{den}}$, respectively. The main message is that reducing the strength of the feedforward connection mostly shifts the f - I curve to the right, while reducing the strength of the feedback connection reduces the gain (Supp. Fig. M5). The dominant shift in changing the feedforward connection is a consequence of the high threshold value θ_0 for eliciting a

calcium spike. Although the feedforward connection strength multiplicatively scales the $\log S$ axis, the main effect is a shift due to the high threshold (Supp. Fig. M6). It is important to note that this shift arises from the model (while also present in the data) because we matched the calcium spike threshold θ_0 to a physiological value ($\theta_0 = 500$ pA, see Larkum et al, 2004). It would also be possible to reproduce the gain modulation by changing the feedforward strength, but at the price of setting the threshold unphysiologically to zero and not being able to reproduce the shift observed with L5 GABAzine application (see below).



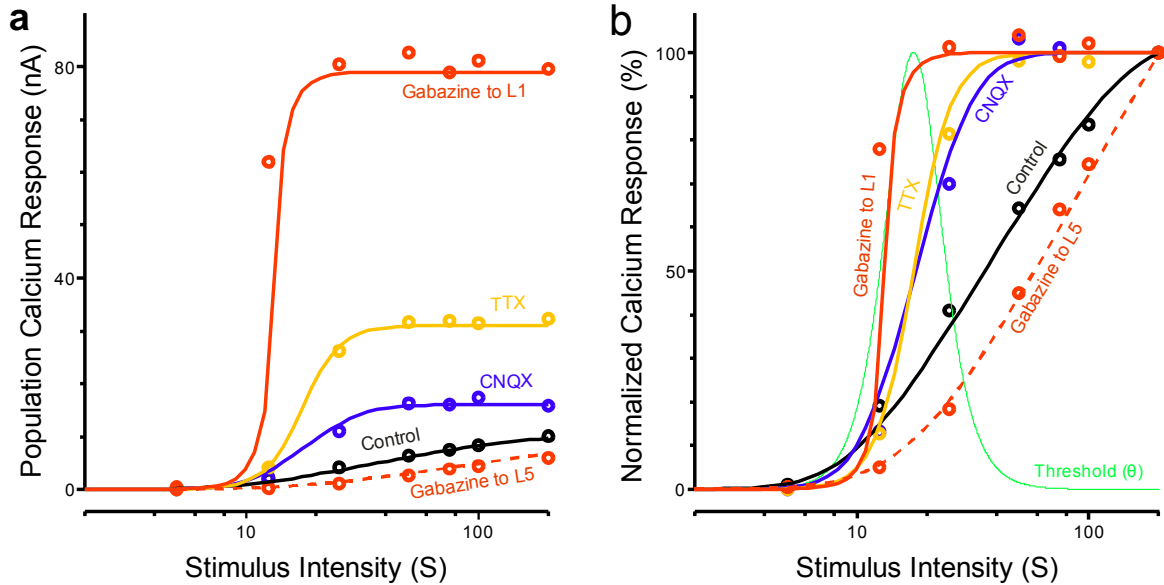
Supplementary Figure M5. Effects of varying the feedforward and feedback connection strengths. **a**, Increasing the feedforward strength by decreasing the feedforward excitation on the Martinotti cell $\alpha_{ex}^{ff\ M}$ leads to mainly a left shift. Solid lines show the solution of the recurrent Eq. 14, and dashed lines the fits using Eq. 15 (values of $\alpha_{ex}^{ff\ M}$ from left to right: 3.04, 1.52, 0 S·(A·s)⁻¹). **b**, Increasing the inhibitory feedback strength $\alpha_{inh}^{fb\ den}$ (describing the inhibitory connection strengths from the Martinotti cells to the pyramidal cell dendrites) leads to an effective gain decrease γ and a simultaneous right shift by θ_i (see Eq. 16 and the definitions in Eqs 12 and 13). Solid lines: solutions of Eq. 14, dashed lines: approximations by Eq. 15 (values of $\alpha_{inh}^{fb\ den}$ from left to right: 28, 14, 0 pA·s). The bell-shaped curve represents the threshold density $\rho\theta$ with $\theta = (\log S)/\beta^f$ and $\beta^f = 1.7 \cdot 10^{-7}$. The black curves in **a**) and **b**) correspond to the control conditions in Fig. 4d of the main text. Similarly, the blue and pink curves in **a**) and **b**) correspond to curves labeled by “No FF_i” and “No FB_i” in Fig. 4d.



Supplementary Figure M6. Differential effect of changing the feedforward and feedback connection strength. **a**, An increase in the feedforward connection strength β^f is equivalent to a scaling of the $\log S$ axis (see Eq. 15). In the presence of a positive threshold θ_0 this also reduces the effective activation threshold. For the measured values of the calcium spike threshold θ_0 the apparent change consists in mainly a threshold shift. **b**, An increase in the feedback connection strength β^b induces a pure gain modulation. The threshold is not affected because the feedback is only manifested when there is already some calcium signal, while it is absent if the calcium threshold is not exceeded.

Explanation of the blocking experiments.

We modeled the local blocking of (1) AMPA receptors in layer 5 by CNQX, (2) action potentials in layer 5 by TTX, and GABA_A receptors by GABAzine (3) in upper cortical layers L1 and (4) in the deep layer L5. The first three blocking experiments (CNQX, TTX, GABAzine in L1) are assumed to disinhibit dendritic calcium receptors in layer 5 pyramidal cells, and thus increase the maximum calcium response given by the product Nc . They are also assumed to weaken the effective feedback strength by shifting β^b towards positive values, while the effective feedforward strength β^f remains roughly unchanged (see Suppl. Figs. M4, M7 and Table 1, 2). Since the calcium spike mechanism can be blocked by specific inhibition in an all-or-none fashion, we assumed that the unit calcium event c remained unchanged while the number of available pyramidal neurons N in which dendritic calcium spikes can be triggered is changed. Hence, the three parameters which were used to fit the four blocking experiments were β^f , β^b , and N (see Table 1 and 2 and Fig. M7). Note that among these 3 parameters, only 2 were considerably changed (β^b and N) while the third (β^f) remained roughly constant.



Supplementary Figure M7: Modeling the effects of CNQX, TTX and Gabazine to L1 and L5 according to the scheme in Fig. M4. **a**, Calcium response function $C(S)$ obtained from solving Eq. 14 and using the parameter values given in Table 1. **b**, Normalized data from **a**). Note that Gabazine to L5 does not change the gain, consistent with the interpretation that in L5 it only affects feedforward projections. All other blocking experiments, in contrast, increase the overall feedback connections and thus lead to a gain increase compared to control. The bell-shaped curve is showing the density $\rho\theta$ with $\theta = (\log S)/\beta^f$ and $\beta^f = 1.7 \cdot 10^{-7}$.

Detailed fitting procedure

The values for the parameters c , θ_0 , R_m^{som} , R_m^{den} , R_T , Θ , and g arising in Table 1 are extracted from the data published in Larkum et al. (2004). From these we calculated the dendritic leak factors λ^{den} and λ^{som} (see Table 2). To obtain the fits in Fig. M7 we first considered the TTX experiment where all connections except the excitatory feedforward inputs to the dendrites (α^{ffden}) are put to 0 (cf. Fig. M4). In this case the calcium signal takes the form $C(S) = Nc/(1+\exp(-(\beta^f \log S - \theta_0)/\sigma))$ with $\beta^f = (1-\lambda^{den})\alpha^{ffden}$ (see Eqs 15 and 12, 13). By fitting this function to the data we extracted the TTX-specific values for α^{ffden} and N . We also extracted the value of σ characterizing the width of the calcium threshold distribution which was then fixed also for the other four response curves.

The data of the remaining experiments (control, CNQX, GABazine in L1, GABazine in L5) were fitted by optimizing the parameters β^f , β^b , and N appearing in Eq. 14 for each experiment separately. From the effective connection strengths β^f and β^b we calculated the physiological connection strengths α^{ffden} , α^{ffsom} and α^{bden} by using the formulas following Eqs 12 and 13. Assuming the blocking patterns specified by the factors in Table 1 one can now uniquely decompose α^{ffden} , α^{ffsom} and α^{bden} into the components specified in Table 1 (see also the formulas in Table 2).

Parameters of the full model	Units	Control (value)	CNQX (factor)	TTX (factor)	Gabazine L1 L5 (factors)	
N (number of pyramidal dendrites generating the population signal)	no un.	10	1.6	3.1	7.9	1
α_{ex}^{bden} (excitat. dendritic feedback strength)	pA·s	6	1	0	1	1
α_{inh}^{bden} (inhibit. dendritic feedback strength)	pA·s	28	0.4	0	0	1
α_{ex}^{ffM} (exc. feedforw. str. to Martinotti cell)	S·(A·s) ⁻¹	1.52	0.4	0	1	1

α_{inh}^{ffM} (inhib. feedfor. str. to Martinotti cell)	$S \cdot (A \cdot s)^{-1}$	1.75	1	0	1	0
α_{ex}^{ffsom} (excit. somatic feedforward strength)	pS	20	0.4	0	1	1
α_{inh}^{ffsom} (inhib. somatic feedforward strength)	pS	10	0.4	0	1	0
α_{ex}^{ffden} (excitat. dendritic feedfor. strength)	pS	240				
c (unit dendrite calcium signal)	pA	100				
θ_0 (mean calcium threshold)	pA	500				
σ (half-width of θ -distribution)	pA	33				
R_m^{som} (som. membrane resist.)	M Ω	50				
R_m^{den} (dendr. membr. resistance)	M Ω	43				
R_T (transfer resistance)	M Ω	65				
Θ (action potential threshold)	pA	200				
g (gain of f - I transfer function)	$(pA \cdot s)^{-1}$	0.07				

Table 1: Parameters of the full model used in Suppl. Fig. M7 and their physiological interpretation. The columns “CNQX”, “TTX”, “GABA_A L1” and “GABA_A L5” give the factors with which the control value is multiplied to mimic the pharmacological interventions as depicted in Suppl. Fig. M4. Given the pattern of blocking factors, we tuned the values of first 7 parameters in the control column to fit the 5 response functions (each characterized by 3 parameters). The remaining parameters (except σ) were extracted from Larkum et al. (2004). Note that N is a nonlinearly increasing function of the feedback connection strength α^{fbden} and roughly a linearly increasing function of the gain factor γ (see Table 2).

Parameters of the analytically reduced model	Units	Control	CNQX	TTX	Gabazine	
					L1	L5
α^{fbden} (feedback strength to den)	pA·s	-22.0	-5.2	0.0	6.0	-22.0
$\alpha^{fbden} = \alpha_{ex}^{fbden} - \alpha_{inh}^{fbden}$						
α^{ffden} (feedforward strength to den)	pA·s	246.4	252.8	240.0	240.0	197.4
$\alpha^{ffden} = \alpha_{ex}^{ffden} - \alpha_{inh}^{fbden} (\alpha_{ex}^{ffM} - \alpha_{inh}^{ffM})$						
α^{ffsom} (feedforw. strength to soma)	pA·s	10	0.8	0	0.1	0.2
$\alpha^{ffsom} = \alpha_{ex}^{ffsom} - \alpha_{inh}^{ffsom}$						
β^f (effect. feedforw. str. to dendrite)	pA·s	124.2	168.6	147.7	202.8	96.8
β^b (effect. feedback str. to dendrite)	no un.	-215.0	-65.5	0.0	93.3	-215.0
λ^{den} (dendritic leak factor)	no un.			0.2722		
λ^{som} (somatic leak factor)	no un.			0.3165		
γ (gain factor of response function)	no un.	0.38	0.67	1.0	3.47	0.38
θ_i (additional shift of calcium thresh.)	pA	-50.49	-15.41	0	22.06	-50.49

Table 2: Derived parameters of the model, calculated from the values in Table 1. The parameters α give the compound connection strengths, while β^f and β^b yield the effective feedforward and feedback connection strengths, $\beta^f = FF_e - FF_i$ and $\beta^b = FB_e - FB_i$, in the reduced model (Eqs 14 – 16 and Suppl. Fig. M3, calculated from the formulas following Eqs 12 and 13). The dendritic and somatic leak factors λ^{den} and λ^{som} are calculated from the passive neuronal parameters according to the formulas following Eq. 3. For the definition of γ and θ_i see Eq. 16.

Bibliography

Larkum M, Senn, W and Lüscher H-R (2004), “Top-down dendritic input increases the gain of layer 5 pyramidal neurons.”, *Cerebral Cortex*, 14:1059-1070

Pérez-Garci E, Gassmann M, Bettler B, Larkum ME. (2006), “The GABAB1b isoform mediates long-lasting inhibition of dendritic Ca^{2+} spikes in layer 5 somatosensory pyramidal neurons.” *Neuron*. 18;50(4):603-16.

ⁱ **Somato-dendritic voltage interactions.** The total dendritic and somatic steady state currents are obtained from solving the coupled differential equations governing the somatic and dendritic voltages,

$$C dV^{som}/dt = -V^{som}/R_m^{som} + I_{syn}^{som}(S) + (V^{som} - V^{den})/R_T$$

$$C dV^{den}/dt = -V^{den}/R_m^{den} + I_{syn}^{den}(S) + c_i(S) + (V^{den} - V^{som})/R_T .$$

Setting the derivatives to 0 and abbreviating $I^{som} = V^{som}/R_m^{som}$ and $I^{den} = V^{den}/R_m^{den}$ (while suppressing the index i), we can solve for these quantities and get (6) as well as

$$I_i^{den}(S) = \lambda^{som} I_{syn}^{som}(S) + (1 - \lambda^{den})(I_{syn}^{den} + c_i(S)) \quad (6')$$

with λ^{som} and λ^{den} defined below Eq. 3. Considering Eqs (6) and (6') together we recognize Kirchhoff's law, stating here that the total membrane current is preserved in the two electrotonically coupled compartments.

ⁱⁱ **Integration of the population calcium signal.** The last expression in (9) is obtained by noticing that the derivative of the second integral with respect to I_0^{den} is $Nc\rho I_0^{den}$. To calculate this derivative we use that the derivative of the step-function Θ is a δ -function. But $Nc\rho I_0^{den}$, with ρ defined in (8), is also the derivative of the last expression in (9) with respect to I_0^{den} .

³ **Parameter identification for the population calcium response as a sigmoidal.** To calculate the additional shift θ_l of the sigmoidal approximation of $C(S)$ (see Eqs 14 and 15) we note that the total shift of the function $C(S)$ along the $s = \beta^{ff} \log S$ axis corresponds to the value of s where the function $C(S)/N$ defined by Eq. 14 (after division by N) reaches its half maximum, i.e. $C(S)/N = c/2$. Replacing $C(S)/N$ with $c/2$ on the right-hand-side of Eq. 14 yields the condition $s + \beta^{fb}(c/2 - \Theta/\lambda^{den}) - \theta_0 = 0$ on s for $C(S)/N$ reaching this half maximum. Equating this with the ansatz in (15) gives $s + \beta^{fb}(c/2 - \Theta/\lambda^{den}) - \theta_0 = s - (\theta_0 + \theta_1)$, from where we get $\theta_1 = \beta^{fb}(\Theta/\lambda^{den} - c/2)$ as defined in (16).

To calculate the additional gain factor γ of the sigmoidal approximation of $C(S)$ we first consider the derivative of C given in (14) with respect to $s = \beta^{ff} \log S$ at the point where C reaches the half maximum $Nc/2$. This derivative is calculated to be $C' = (1 + \beta^{fb} C'/N) \cdot Nc/(4\sigma)$. Solving for C' yields $C' = \gamma Nc/(4\sigma)$ with additional gain factor $\gamma = (1 - \beta^{fb} c/(4\sigma))^{-1}$ as defined in (15) and (16).